Stabilities and fragmentation energies of Si_n clusters (n = 2–33)

2009 J. Phys.: Condens. Matter 21 455501

(http://iopscience.iop.org/0953-8984/21/45/455501)

J. Phys.: Condens. Matter **21** (2009) 455501 (7pp) doi:10.1088/0953-8984/21/45/455501

Stabilities and fragmentation energies of Si_n clusters ($n = 2$–33)

Wei Qin[1], Wen-Cai Lu[1,2], Li-Zhen Zhao[2], Qing-Jun Zang[3], C Z Wang[4] and K M Ho[4]

[1] State Key Laboratory of Theoretical and Computational Chemistry, Institute of Theoretical Chemistry, Jilin University, Changchun, Jilin 130021, People's Republic of China
[2] Laboratory of Fiber Materials and Modern Textile, The Growing Base for State Key Laboratory, and College of Physics, Qingdao University, Qingdao 266071, People's Republic of China
[3] College of Chemistry, Beijing Normal University, Beijing 100875, People's Republic of China
[4] Ames Laboratory–US DOE and Department of Physics and Astronomy, Iowa State University, Ames, IA 50011, USA

E-mail: wencailu@jlu.edu.cn

Received 12 June 2009, in final form 12 September 2009
Published 21 October 2009
Online at stacks.iop.org/JPhysCM/21/455501

Abstract

The structures of Si_n ($n = 2$–33) were confirmed by genetic algorithm (GA)/tight binding (TB) search and *ab initio* calculations at the B3LYP/6-311 + +G(2d) and PW91/6-311 + +G(2d) level, respectively. The fragmentation energies, binding energies, second differences in energy, and highest occupied molecular orbital (HOMO)–lowest unoccupied molecular orbital (LUMO) gaps in the size range $2 \leqslant n \leqslant 33$ were calculated and analyzed systematically. We extended the cluster size involved in the fragmentation analyses up to Si_{33}, and studied the multi-step fragmentations of Si_n. The calculated result is similar to the fragmentation behavior of small silicon clusters studied previously, showing that Si_6, Si_7, and Si_{10} have relatively larger stabilities and appear more frequently in the fragmentation products of large silicon clusters, which is in good agreement with the experimental observations.

(Some figures in this article are in colour only in the electronic version)

1. Introduction

Over the past several decades, cluster science has undergone intensive development. Cluster research is primarily driven by the interest in evolution of the structures and properties of materials from molecular to macroscopic systems. In particular, semiconductor clusters have attracted considerable experimental [1–23] and theoretical [24–39] interest largely because of their potential applications in the microelectronics industry. Among these semiconductor clusters silicon clusters have attracted most attention. Earlier experiments [11, 16, 19, 20] revealed a structural transition from prolate to near-spherical geometry in the size range of 24–34 for both cationic and anion silicon clusters, and the size range of $n \geqslant 25$ has received increasing attention. In order to obtain a better understanding of the properties of silicon microparticles it is of both fundamental and practical interest to investigate the structures and properties of small-to-medium-sized clusters [35]. Extensive studies have been performed on the geometric structures of low-energy silicon clusters along with a search for their growth pattern [32, 40, 41]. For example, Yoo *et al* reported a series of geometric structures of silicon clusters [32, 41]. They found a new growth pattern of 'Y-shaped' three-armed structures when $n \geqslant 26$, where each arm is a small-sized magic cluster (Si_6, Si_7 or Si_{10}) [32], and classified the geometric structures of silicon clusters into four families in the size range $n \leqslant 29$. They also constructed stuffed-fullerene clusters and obtained more spherical-like Si_n geometric structures in the size range 27–39 using a genetic algorithm (GA) combined with the tight-binding (TB) method [30]. Recently, Yoo and co-workers [32, 33] performed an unconstrained search for the low-energy structures of medium-sized silicon clusters Si_{21}–Si_{40} and Si_{45} by means of the minimum-hopping global optimization method coupled with a density functional based tight-binding (DFTB) model of silicon, followed by first principles DFT calculations to determine the relative stability of various candidate low-energy

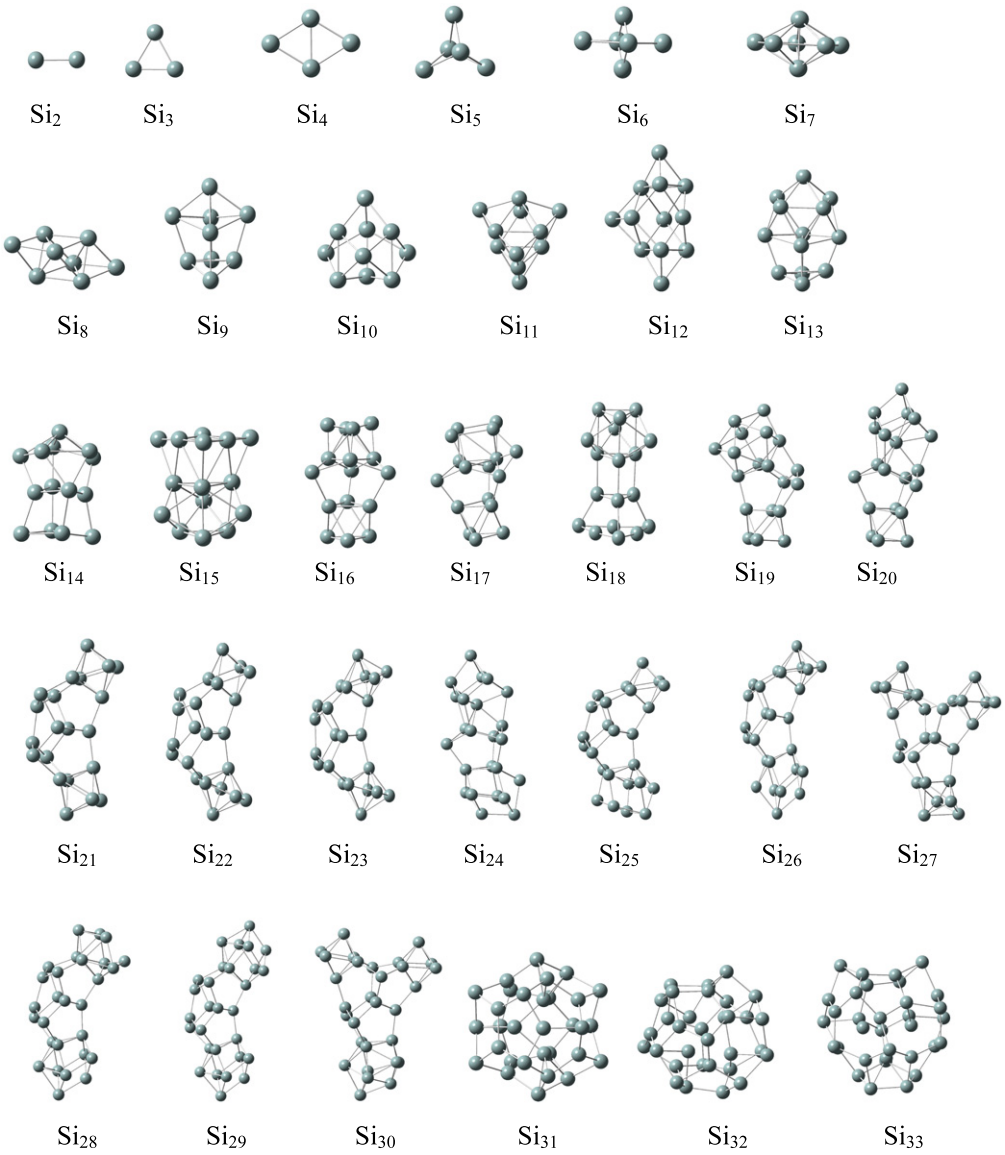

Figure 1. Lowest-energy structures of Si_n ($n = 2$–33) clusters.

silicon clusters. Oña *et al* reported considerable structures with lower energies that are different from the previous studies [34]. They employed a GA with the MSINDO semi-empirical molecular orbital method to search for stable structures in the size range Si_{18}–Si_{60} and further optimized the structures using density functional theory.

Although the geometric structures of silicon clusters have been studied extensively in the literature, studies of their properties, especially their fragmentation behaviors, are much less common. Using a photo-ionization mass spectrum experiment [42], it is shown that medium-sized silicon clusters can be separated into small-sized clusters, in which Si_6, Si_7, Si_9 and Si_{10} appear more frequently than other small clusters. Computational studies of the fragmentation behavior of Si_n clusters have been performed by Raghavachari's group [43] and Ho's group [44]. The fragmentation energies for Si_n ($n = 2$–10) and Si_n ($n = 2$–20) were reported, respectively. In this paper, a relatively larger cluster size range of Si_n ($n = 2$–33) is considered in our fragmentation calculation, and the statistical results of fragmentation behaviors should be more accurate. We recalculated and verified all the lowest-energy structures of silicon clusters for $n \leqslant 33$ by GA search with the TB method and *ab initio* calculations at the level of B3LYP/6-311++G(2d) and PW91/6-311++G(2d) using the GAUSSIAN 03 software package. Then, we systematically studied their fragmentation energies as well as their binding energies, second differences in energy, and highest occupied molecular orbital (HOMO)–lowest unoccupied molecular orbital (LUMO) gaps as the function of cluster size. The binding energy behaviors can help us determine the relative stabilities of clusters, and the second differences in energy can show clearly the cluster with larger stability compared with their nearest neighbors. HOMO–LUMO gaps can suggest the reaction stabilities of silicon clusters. For the first time we extend the size of the Si cluster in the fragmentation energy calculation up to Si_{33}, and study the multi-step fragmentations

Table 1. Binding energies, second differences in energy ($\Delta^2 E$), and HOMO–LUMO gaps of Si_n ($n = 2$–33) clusters, optimized at the B3LYP/6-311 + +G(2d) and PW91/6-311 + +G(2d) levels.

	E_b (eV)		$\Delta^2 E$ (eV)		HOMO–LUMO gaps (eV)	
Si_n	B3LYP	PW91	B3LYP	PW91	B3LYP	PW91
1	0	0				
2	1.598 71	1.748 66	−0.552 06	−0.765 69	1.719 50	0.391 03
3	2.315 63	2.586 77	−0.463 67	−0.330 29	2.220 19	1.042 75
4	2.790 01	3.088 40	0.697 46	0.333 57	2.416 93	1.137 99
5	2.935 15	3.322 66	−0.371 91	−0.166 33	3.184 03	2.040 05
6	3.093 89	3.506 56	0.124 49	0.055 21	3.212 87	2.082 78
7	3.189 49	3.630 03	1.171 66	1.286 30	3.156 82	2.093 93
8	3.114 74	3.561 84	−1.136 85	−1.315 15	2.575 85	1.469 70
9	3.182 91	3.654 94	−0.260 14	−0.295 57	2.929 87	1.955 97
10	3.263 47	3.758 97	1.375 29	1.617 39	3.045 79	2.080 05
11	3.204 35	3.697 01	−0.868 52	−0.966 73	2.776 94	1.714 33
12	3.227 46	3.726 01	0.848 97	0.900 67	3.213 15	2.206 04
13	3.181 71	3.688 93	−1.487 39	−1.440 28	1.810 93	0.856 08
14	3.248 74	3.760 02	0.573 24	0.574 02	2.754 63	1.776 65
15	3.268 61	3.783 37	0.255 21	0.705 16	3.112 19	2.163 32
16	3.270 05	3.759 72	−0.441 72	−0.670 65	2.098 83	1.099 08
17	3.297 31	3.778 31	0.618 44	−0.140 93	2.425 10	1.382 89
18	3.287 17	3.802 66	−0.456 57	0.379 44	2.756 54	1.885 22
19	3.302 14	3.804 47	−0.234 45	−0.304 41	2.212 30	1.300 71
20	3.327 33	3.821 33	−0.074 82	0.048 11	2.735 85	1.756 78
21	3.353 68	3.834 29	0.750 72	0.439 53	2.639 53	1.658 55
22	3.343 52	3.826 01	0.043 04	0.068 51	2.803 07	1.836 78
23	3.332 37	3.815 63	−0.492 63	−1.035 25	2.745 11	1.709 70
24	3.342 67	3.849 17	−0.291 70	0.517 50	2.691 23	1.720 05
25	3.363 82	3.859 33	0.689 89	0.415 73	2.540 20	1.622 63
26	3.356 80	3.852 72	0.011 67	0.366 53	2.383 46	1.474 32
27	3.349 88	3.833 02	−0.325 72	−1.267 95	2.499 66	1.541 27
28	3.355 08	3.860 02	−0.395 51	0.190 03	1.763 04	0.763 01
29	3.373 56	3.878 60	0.739 22	1.099 68	2.352 44	1.426 43
30	3.366 16	3.859 28	0.264 18	−0.649 16	2.222 10	1.298 00
31	3.350 73	3.862 15	−0.135 21	−0.397 58	1.436 77	0.610 08
32	3.340 48	3.877 27	−1.020 82	−0.096 22	1.325 75	0.662 06
33	3.361 79	3.894 39			1.550 24	0.743 97

of Si_n. The behaviors of the calculated fragmentation energies are in good agreement with the experimental observations [42].

2. Computational method

The computational process can be divided into three steps. Firstly we repeated and verified the lowest geometric structures of silicon clusters Si_{2-18} from the literature [25, 32, 41, 45–48] with first principles calculations at the two levels of B3LYP/6-311 + +G(2d) and PW91/6-311 + +G(2d). Secondly we searched for the lowest-energy structures of silicon clusters in the range of $19 \leqslant n \leqslant 33$ by the GA method with the TB potential, and the selected candidates were further optimized using the all-electron DFT method at the B3LYP/6-311 + +G(2d) and PW91/6-311++G(2d) levels. The lowest-energy structures obtained from our study agree with those reported in the literature [25, 32, 49]. The GA method is frequently used in searching for low-energy structures when the cluster size gets larger. Its principle and operational procedure can be found in many works, e.g. in [50] and [51]. Finally, the binding and fragmentation behaviors of the clusters were studied using the lowest-energy structures of the clusters. All of the first principles calculations were performed with the GAUSSIAN 03 software package.

3. Results and discussions

Figure 1 shows the lowest-energy isomers of Si_n clusters ($n \leqslant 33$). All of the structures were confirmed to be at energy minima because all the vibration frequencies are real from frequency analysis. Very small Si_n clusters ($n \leqslant 4$) have a plane configuration, i.e. Si_3 and Si_4, have triangle and rhombus structures, respectively. When n reaches 5, Si_n clusters show three-dimensional structures, e.g. the structures of Si_5, Si_6, and Si_7 are trigonal bipyramid, edge capped trigonal bipyramid, and pentagonal bipyramid, respectively. For Si_n ($8 \leqslant n \leqslant 30$), the geometries favor prolate structures, and the structures for $n \geqslant 19$ consist of two or three stable clusters. These stable clusters are connected via a Si_6 or Si_9 unit, both of which are segments of diamond. In our calculations, when n reaches 31, the structures of Si_n would transform into cages. In fact, in the size range around the transition point, the stabilities of prolate and cage structures compete with each other, and their binding energies are very close.

3.1. Analyses of binding energies, second differences in energy, and HOMO–LUMO gaps of Si_n ($n = 2$–33)

In order to understand the relative stabilities of Si_n clusters we have analyzed the binding energies per atom,

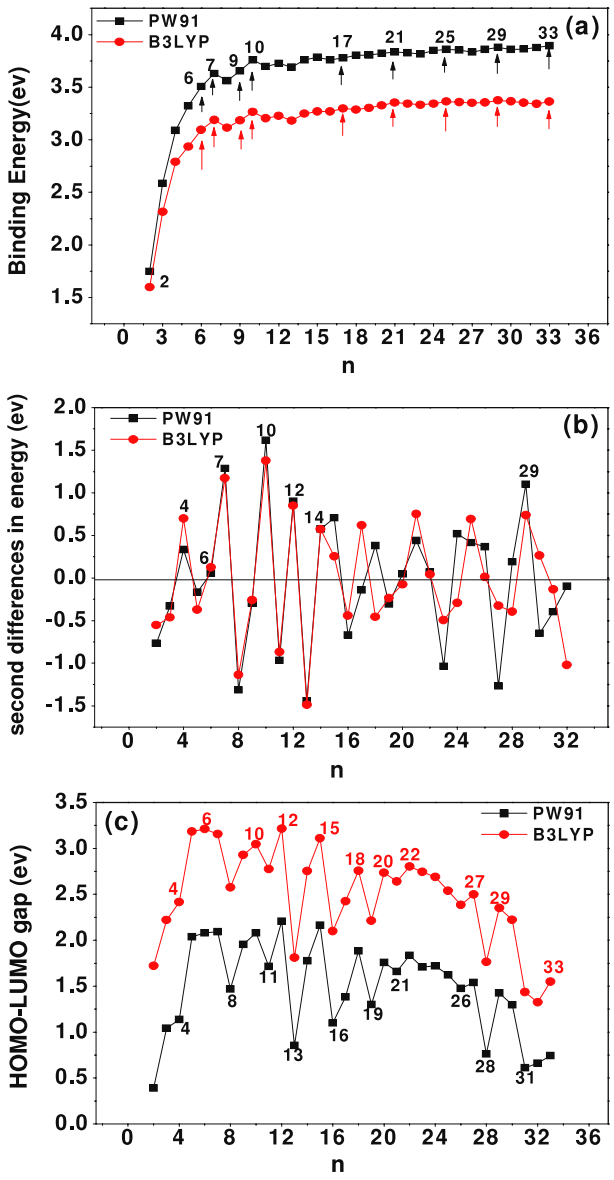

Figure 2. (a) Binding energies per atom of Si_n clusters as a function of cluster size. (b) Plot of second differences in total energy as a function of cluster size, defined by $\Delta^2 E = [E(Si_{n+1}) + E(Si_{n-1}) - 2E(Si_n)]$. (c) The HOMO–LUMO gaps of Si_n clusters as a function of cluster size.

second differences in energy, and the highest occupied molecular orbital (HOMO)–lowest unoccupied molecular orbital (LUMO) gaps of the clusters as a function of cluster size, based on the lowest-energy structures. For all of the selected candidates, we further optimized them using two DFT functionals: the B3LYP and PW91 functionals with the 6-311 + +G(2d) basis set in the GAUSSIAN 03 package [52]. The calculation results are summarized in table 1, and are plotted in figures 2–4.

The binding energy per atom $BE(Si_n)$ is defined as

$$BE(Si_n) = [nE(Si) - E(Si_n)]/n \quad (1)$$

where $E(Si)$ and $E(Si_n)$ are the energy of a single Si atoms and that of a n-atom cluster, respectively. Figure 2(a) shows the

Table 2. Fragmentation energies of Si_n clusters optimized at the B3LYP/6-311 + +G(2d) level. The fragmentation energies in bold indicate the easiest fragmentation channels.

Si_n	$Si_p + Si_{n-p}$	E_f	Si_n	$Si_p + Si_{n-p}$	E_f
2	$Si_1 + Si_1$	**3.197**	19	$Si_{10} + Si_9$	**1.4615**
3	$Si_1 + Si_2$	**3.75**	19	$Si_{12} + Si_7$	1.6847
4	$Si_1 + Si_3$	**4.2134**	20	$Si_{10} + Si_{10}$	**1.2755**
4	$Si_2 + Si_2$	4.7652	21	$Si_{11} + Si_{10}$	**2.5443**
5	$Si_1 + Si_4$	**3.5158**	21	$Si_{14} + Si_7$	2.6186
5	$Si_2 + Si_3$	4.5314	22	$Si_{12} + Si_{10}$	**2.1856**
6	$Si_1 + Si_5$	**3.8845**	22	$Si_{15} + Si_7$	2.2018
6	$Si_4 + Si_2$	4.2059	22	$Si_{16} + Si_6$	2.6732
6	$Si_3 + Si_3$	4.6789	23	$Si_{16} + Si_7$	**1.9863**
7	$Si_1 + Si_6$	**3.765**	23	$Si_{17} + Si_6$	2.0269
7	$Si_3 + Si_4$	4.2195	24	$Si_{17} + Si_7$	**1.8401**
8	$Si_1 + Si_7$	**2.5925**	24	$Si_{14} + Si_{10}$	2.1071
8	$Si_4 + Si_4$	2.5978	25	$Si_{15} + Si_{10}$	**2.4314**
9	$Si_5 + Si_4$	**2.81**	25	$Si_{21} + Si_4$	2.508
10	$Si_4 + Si_6$	**2.913**	26	$Si_{20} + Si_6$	**2.1623**
11	$Si_4 + Si_7$	**1.7604**	26	$Si_{21} + Si_5$	2.1738
12	$Si_6 + Si_6$	**1.6076**	27	$Si_{21} + Si_6$	**1.4582**
12	$Si_5 + Si_7$	1.7273	27	$Si_{20} + Si_7$	1.5736
13	$Si_6 + Si_7$	**0.475**	27	$Si_{17} + Si_{10}$	1.7578
14	$Si_7 + Si_7$	**0.8304**	28	$Si_{21} + Si_7$	**1.1891**
15	$Si_5 + Si_{10}$	**1.7139**	29	$Si_{22} + Si_7$	**1.9597**
15	$Si_9 + Si_6$	1.8196	30	$Si_{20} + Si_{10}$	**1.7936**
15	$Si_8 + Si_7$	1.7848	30	$Si_{21} + Si_9$	1.9114
16	$Si_{10} + Si_6$	**1.126**	30	$Si_{23} + Si_7$	2.0141
16	$Si_9 + Si_7$	1.3482	31	$Si_{21} + Si_{10}$	**0.8105**
17	$Si_{10} + Si_7$	**1.0961**	32	$Si_{25} + Si_7$	**0.4849**
18	$Si_{11} + Si_7$	**1.5943**	32	$Si_{22} + Si_{10}$	0.7033
18	$Si_8 + Si_{10}$	1.6166	32	$Si_{26} + Si_6$	1.0552
18	$Si_9 + Si_9$	1.8767	33	$Si_{26} + Si_7$	**1.3485**

curve of binding energy per atom as a function of cluster size. We can see that in general the binding energy of Si clusters increases gradually along with the cluster size n. However, according to the binding energies, clusters between $n = 11$ and 20 are not as favorable as those with $n = 7$–10, suggesting that clusters in the size range of $n = 11$–20 are not very stable and would easily dissociate into smaller fragments. To see more clearly the relative stabilities of the clusters, we also calculated the second differences in energy $\Delta^2 E$ for these lowest-energy isomers which are defined by

$$\Delta^2 E = [E(Si_{n+1}) + E(Si_{n-1}) - 2E(Si_n)].$$

Figure 2(b) shows the second differences in energy as a function of cluster size. From the definition of $\Delta^2 E$, it is clear that the clusters with larger positive values of $\Delta^2 E$, are more stable than their nearest neighbors. Local maximum peaks for $\Delta^2 E$ are found at $n = 4$, 7, 10, 12, and 14, indicating that the clusters with these values of n are more stable than their neighboring clusters. This fact has been also reflected in the previous studies of the magic stability pattern of silicon clusters where $n = 4$, 6, 7, 10, and 12 are more stable than their nearest neighbors [53, 54]. Usually the cluster stability is ascribed either to the geometrical close packing model (usually obeyed by inert gas cluster) or the electronic shell model (usually obeyed by alkali metal clusters) [54–56]. In this work, the relatively stable silicon clusters with $n = 4$, 7, 10, 12, and 14, may be mainly due to a steric effect.

Table 3. Fragmentation energies of Si_n clusters optimized at the PW91/6-311 + +G(2d) level. The fragmentation energies in bold indicate the easiest fragmentation channels.

Si_n	$Si_p + Si_{n-p}$	E_f	Si_n	$Si_p + Si_{n-p}$	E_f
2	$Si_1 + Si_1$	**3.4976**	19	$Si_{10} + Si_9$	**1.8003**
3	$Si_1 + Si_2$	**4.2632**	19	$Si_{12} + Si_7$	2.1626
4	$Si_1 + Si_3$	**4.592**	20	$Si_{10} + Si_{10}$	**1.2489**
4	$Si_2 + Si_2$	5.3590	21	$Si_{11} + Si_{10}$	**2.2653**
5	$Si_4 + Si_1$	**4.2615**	21	$Si_{14} + Si_7$	2.4695
5	$Si_3 + Si_2$	5.3557	22	$Si_{12} + Si_{10}$	**1.8733**
6	$Si_1 + Si_5$	**4.4243**	22	$Si_{15} + Si_7$	2.0133
6	$Si_4 + Si_2$	5.5185	22	$Si_{16} + Si_6$	2.9791
6	$Si_3 + Si_3$	5.5187	23	$Si_{16} + Si_7$	**2.1989**
7	$Si_1 + Si_6$	**4.3711**	23	$Si_{17} + Si_6$	2.4888
7	$Si_3 + Si_4$	5.2963	24	$Si_{14} + Si_{10}$	**2.1457**
8	$Si_1 + Si_7$	**3.089**	24	$Si_{17} + Si_7$	2.7387
8	$Si_4 + Si_4$	3.7875	25	$Si_{15} + Si_{10}$	**2.1324**
9	$Si_5 + Si_4$	**3.9294**	25	$Si_{21} + Si_4$	3.6096
10	$Si_4 + Si_6$	**4.2017**	26	$Si_{16} + Si_{10}$	**2.4247**
11	$Si_4 + Si_7$	**2.9063**	26	$Si_{20} + Si_6$	2.7048
12	$Si_6 + Si_6$	**2.6373**	27	$Si_{20} + Si_7$	**1.6541**
12	$Si_5 + Si_7$	2.6886	27	$Si_{17} + Si_{10}$	1.6707
13	$Si_6 + Si_7$	**1.508**	27	$Si_{21} + Si_6$	1.9322
14	$Si_7 + Si_7$	**1.8202**	28	$Si_{18} + Si_{10}$	**2.0394**
15	$Si_5 + Si_{10}$	**2.5509**	28	$Si_{21} + Si_7$	2.1502
15	$Si_9 + Si_6$	2.8167	29	$Si_{19} + Si_{10}$	**2.5974**
15	$Si_8 + Si_7$	2.8455	29	$Si_{22} + Si_7$	2.8951
16	$Si_{10} + Si_6$	**1.5279**	30	$Si_{20} + Si_{10}$	**1.7471**
16	$Si_9 + Si_7$	1.8509	30	$Si_{21} + Si_9$	2.3640
17	$Si_{10} + Si_7$	**1.2356**	31	$Si_{21} + Si_{10}$	**1.6143**
18	$Si_8 + Si_{10}$	**2.3583**	32	$Si_{25} + Si_7$	**2.1723**
18	$Si_{11} + Si_7$	2.3700	32	$Si_{22} + Si_{10}$	2.3090
18	$Si_9 + Si_9$	2.6589	33	$Si_{26} + Si_7$	**2.9429**

The HOMO–LUMO gaps can reflect the reactive stability at some level. As is well known, the HOMO–LUMO gap of a metal is zero, while nonmetals have definite gaps. Generally, a higher-energy gap would make the clusters more stable and more abundant. The HOMO–LUMO gap as a function of silicon cluster size is shown in figure 2(c), from which we can see that a local maximum peak appears at $n = 6$, indicating the large reactive stability of Si_6. In addition, Si_7, Si_{10}, Si_{12}, and Si_{14}, which have high binding energies, also exhibit relatively large HOMO–LUMO gaps. Note that after the structural transition at $n = 30$, i.e. Si_{31}, Si_{32} and Si_{33}, the clusters have much smaller HOMO–LUMO gaps than those with $n \leqslant 30$, which can be ascribed to the transition of structural motif from prolate to cage at $n = 30$. Thus, cages may have strong reactivity, either easily dissociating into smaller clusters or readily combining with each other into larger ones. In addition, the HOMO–LUMO gap of Si_n clusters generally decreases as cluster size n increases, suggesting that larger clusters would be more reactive.

3.2. Fragmentation behavior

3.2.1. One-step fragmentation. We have calculated one-step fragmentation energies for Si_n clusters. The results are listed in tables 2 and 3. Also we chose the ground states of small Si clusters by considering the spin states. The fragmentation energy values in bold denote the easiest fragmentation channels. As is known, the fragmentation processes may involve dissociation barriers. For simplicity, we predicted the fragmentation paths from a thermodynamic viewpoint, i.e. only considering the fragmentation energies (the total energy differences between reactants and products) which can be expressed as

$$E_f(Si_n) = E(Si_{n-p}) + E(Si_p) - E(Si_n). \quad (2)$$

For clarity, we plotted the fragmentation energies for the easiest fragmentation channels as a function of cluster size, as shown in figure 3(a). The larger the fragmentation energies are, the more difficult the dissociations of clusters, and thus the more stable the relevant clusters are. Tables 2 and 3 show that when the silicon clusters decompose into Si_6, Si_7, and Si_{10}, their fragmentation energies are smaller compared to other channels, showing that Si_6, Si_7, and Si_{10} would appear frequently in fragmentation products, which is in agreement

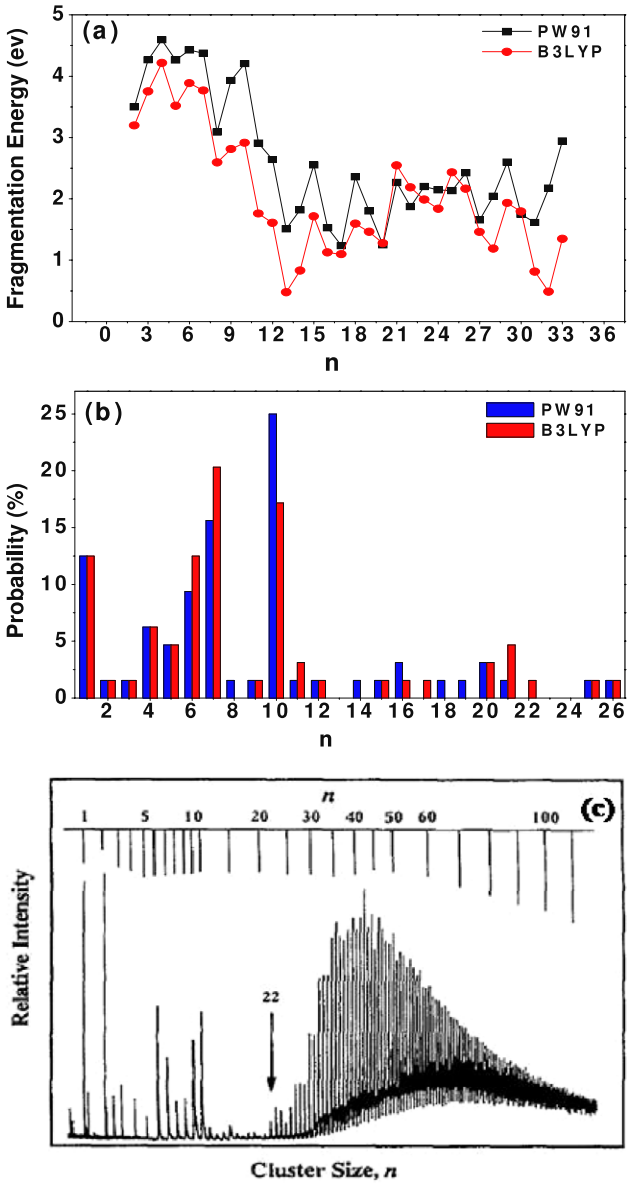

Figure 3. (a) Easiest fragmentation channels of Si_n clusters. (b) Probabilities of fragmentation outputs. (c) Relative intensities of Si_n clusters in the experiment [42].

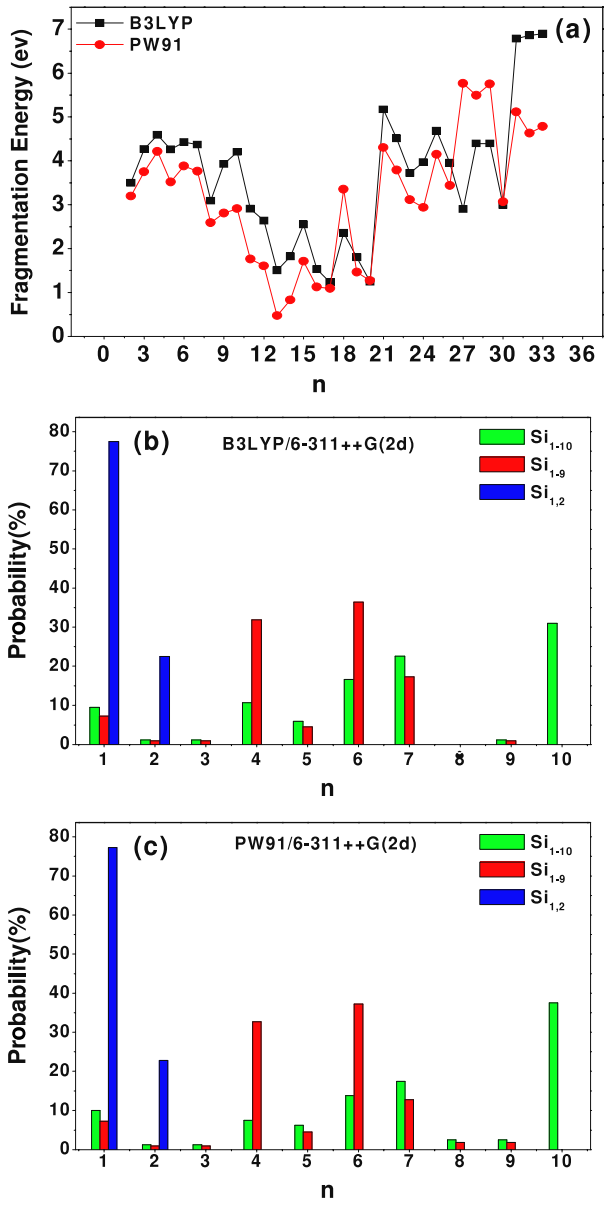

Figure 4. (a) Fragmentation energies of multi-step dissociations of Si_n clusters where Si_n with $n \leqslant 10$ are assumed not to dissociate further. (b) Probabilities of multi-step fragmentation products at the B3LYP/6-311 + +G(2d) level. (c) Probabilities of multi-step fragmentation products at the PW91/6-311 + +G(2d) level.

with the previous studies of fragmentation behaviors of small silicon clusters with $n \leqslant 10$ [43] and $n \leqslant 20$ [44]. Tables 2 and 3 show that the easiest fragmentation channels for the two methods have some differences, the B3LYP calculated results favor the production of Si_6 or Si_7 in the fragmentations, while the PW91 calculated results favor Si_{10} as a dissociated fragment. In the following discussions, we describe the fragmentations of Si clusters mainly based on the B3LYP calculated results. Tables 2 and 3 also show that Si_4, Si_6, Si_7, and Si_{10} are more abundant in the fragmentation products of silicon clusters, which is in agreement with the experimental results [42]. We also present the distribution of fragmentation products as a function of cluster size in figure 3(b), from which Si_4, Si_6, Si_7, and Si_{10} are seen to be dominant products of fragmentations. In their experiment [42], Fuke *et al* reported a photo-ionization mass spectrum for Si_n clusters ($n = 1$–120), from which one can see that for $n \leqslant 33$ the fragmentation products Si_1, Si_2, Si_4, Si_{7-12}, and Si_{29-33} are more abundant. From figures 3(a) and (b) we can see clearly that the probabilities of fragmentation products of Si_1, Si_2, Si_{4-7}, and Si_{10} are larger from our calculations, which is in agreement with the experimental results referred to above. Note that the size range ($n = 2$–33) we used in the present analysis is not large enough to account for the probability of appearances of larger Si clusters ($n \geqslant 29$) in fragmentation products. For the probabilities of the fragmentation products Si_8, Si_9, Si_{11}, and Si_{12}, there are deviations between experimental and theoretical results by comparing figures 3(a) and (b) with figure 3(c). This could be ascribed to two factors: (1) due to the limited size range of Si clusters we used in our analysis, the clusters which could be decomposed to Si_8, Si_9, Si_{11}, and Si_{12} have not been involved adequately and the statistics is poor; (2) as can be seen from tables 2 and 3, there exist several fragmentation channels with almost degenerate fragmentation energies; however, we only consider one fragmentation channel with the smallest fragmentation energy.

When clusters dissociate, which bonds are likely to break is an important question. We can expect that in the fragmentation of clusters, the dissociation of a small stable cluster would be favorable. For example, the calculated results show that when Si_{25} is dissociated into Si_{15} and Si_{10}, the breaking away of the Si_{10} segment from Si_{25} should occur most easily, i.e. the bonds between Si_{10} and Si_{15} may break more easily in $Si_{25} \rightarrow Si_{15} + Si_{10}$. As another example, when Si_{17} is dissociated into Si_{10} and Si_7, the Si_6 unit plus the atom which is nearest to the Si_6 can be considered as a Si_7 fragment, which would break away from the Si_{10} fragment in $Si_{17} \rightarrow Si_{10} + Si_7$.

As is known, the smaller the fragmentation energy of a cluster is, the less stable the cluster will be, i.e. clusters with small fragmentation energies could be easily dissociated. From tables 2 and 3 and figure 3(a) it is found that when $n = 11$ the fragmentation energy curve has a sudden drop, and when n reaches 21 the fragmentation energy rises again. This phenomenon implies that Si_n clusters with $n = 11$–20 are readily dissociated, and this is in good agreement with the experimental results [42].

3.2.2. Multi-step fragmentations. In order to better understand the fragmentation behaviors and make comparison with the experiment results, we further calculated the multi-step fragmentation energies. We adopted three kinds of assumptions: (1) Silicon clusters would decompose sequentially up to $n \leqslant 10$, i.e. the small silicon clusters with $n \leqslant 10$ would not decompose continuously. For example, Si_{30} can decompose into Si_{20} and Si_{10}, in which Si_{20} decompose continuously into $2Si_{10}$s. (2) Silicon clusters would decompose sequentially up to $n \leqslant 9$, i.e. considering $Si_{10} \rightarrow Si_4 + Si_6$ decomposition. (3) All clusters can dissociate sequentially up to Si_1 or Si_2. Again we compared the multi-step fragmentation results with the experiment data. Figures 4(b) and (c) are in general consistent with the experimental observations [42]. If $n \leqslant 10$ clusters are not allowed to dissociate further,

then $Si_{4,6,7,10}$ are shown to be most abundant; If we consider $Si_{10} \rightarrow Si_4 + Si_6$, then the possibilities of Si_4 and Si_6 increase obviously, being close to that of Si_7. Finally, if it is assumed that all clusters can dissociate up to $n \leqslant 2$, then Si_1 is obviously much more abundant than Si_2. Therefore, the yields of Si_4 and Si_6 are apparently related to the yield of Si_{10}, and the output of Si is closely related to the output of Si_{2-8}, which can explain the experimental results that Si and Si_2 have similar yields as do Si_6 and Si_7 at high temperature or with laser irradiation.

4. Conclusion

The geometric structures of Si_n clusters ($2 \leqslant n \leqslant 33$) have been obtained by using a GA search combined with the *ab initio* all-electron DFT method. In this work, we focused on analyzing a series of properties for these silicon clusters including binding energies per atom, second differences in energy, HOMO–LUMO gaps, and especially the fragmentation energies. The stabilities and fragmentation behaviors (involving one-step and multi-step fragmentations) of Si_n clusters were discussed in detail. By analyzing the binding energies and second differences in energy, $Si_{4,7,10,12,14,}$ are shown to have large thermodynamic stability. By analyzing the fragmentation energies for Si_n with $n \leqslant 33$, $Si_{4,6,7,10}$ are shown to be relatively stable species which appear frequently in fragmentation products. In addition, the yields of Si_4 and Si_6 are much enhanced via Si_{10} fragmentation, and the output of Si can reach the output of Si_{2-8} by including Si_n ($n = 2$–8) dissociation into Si_{n-1} and Si atoms. For the size range between 11 and 20, the fragmentation energies are obviously small, indicating that Si_{11-20} can be easily dissociated. Our calculated results are in good agreement with the experimental observations [42].

Acknowledgments

This work was supported by the National Natural Science Foundation of China (nos 20773047 and 60028403). Ames Laboratory is operated for the US Department of Energy by Iowa State University under contract no. DE-AC02-07CH11358. This work was also supported by the Director for Energy Research, Office of Basic Energy Sciences.

References

[1] Gingerich K A, Schmude R W Jr, Baba M S and Meloni G 2000 *J. Chem. Phys.* **112** 7443
[2] Martin T P and Schaber H 1985 *J. Chem. Phys.* **83** 855
[3] Phillips J C 1986 *J. Chem. Phys.* **85** 5246
[4] Schulze W, Winter B and Goldenfeld I 1987 *J. Chem. Phys.* **87** 2402
[5] Heath J R, Liu Y, O'Brien S C, Zhang Q L, Curl R F, Tittel F K and Smalley R E 1985 *J. Chem. Phys.* **83** 5520
[6] Yoshida S and Fuke K 1999 *J. Chem. Phys.* **111** 3880
[7] Burton G R, Xu C S, Arnold C C and Meumark D M 1996 *J. Chem. Phys.* **104** 2757
[8] Hunter J M, Fye J L, Jarrold M F and Bower J E 1993 *Phys. Rev. Lett.* **73** 2063
[9] Alford J M, Laaksonen R T and Smalley R E 1991 *J. Chem. Phys.* **94** 2618
[10] Shvartsburg A A, Liu B, Lu Z Y, Wang C Z, Jarrold M F and Ho K M 1999 *Phys. Rev. Lett.* **83** 2167
[11] Shvartsburg A A, Hudgins R R, Dugourdb P and Jarrold M F 2001 *Chem. Soc. Rev.* **30** 26
[12] Marsen B, Lonfat M, Scheier P and Sattler K 2000 *Phys. Rev.* B **62** 6892
[13] Ray U and Jarrold M F 1991 *J. Chem. Phys.* **94** 2631
[14] Bergeron D E and Castleman A W Jr 2002 *J. Chem. Phys.* **117** 3219
[15] Jarrold M F, Ijiri Y and Ray U 1991 *J. Chem. Phys.* **94** 3607
[16] Jarrold M F, Ijiri Y and Constant V A 1991 *Phys. Rev. Lett.* **67** 2994
[17] Schäfer R, Schlecht S, Woenckhaus J and Becker J A 1996 *Phys. Rev. Lett.* **76** 471
[18] Jarrold M F and Honea E C 1991 *J. Phys. Chem.* **95** 9181
[19] Jarrold M F and Bower J E 1992 *J. Chem. Phys.* **96** 9180
[20] Hudgins R R, Imai M and Jarrold M F 1999 *J. Chem. Phys.* **111** 7865
[21] Zhang Q L, Liu Y, Curl R F, Tittle F K and Smalley R E 1988 *J. Chem. Phys.* **88** 1670
[22] Fuke K, Tsukamoto K, Misaizu F and Sanekata M 1993 *J. Chem. Phys.* **99** 7807
[23] Yoshida S and Fuke K 1999 *J. Chem. Phys.* **111** 3880
[24] Mitas L, Grossman J C, Stich I and Tobik J 2000 *Phys. Rev. Lett.* **84** 1479
[25] Yoo S and Zeng X C 2005 *Angew. Chem. Int. Edn* **44** 1491
[26] Goedecker S and Hellmann W 2005 *Phys. Rev. Lett.* **95** 055501
[27] Sieck A, Frauenheim Th and Jackson K A 2003 *Phys. Status Solidi* b **240** 537
[28] Jackson K A and Horoi M 2004 *Phys. Rev. Lett.* **93** 013401
[29] Yoo S, Zeng X C, Zhu X L and Bai J 2003 *J. Am. Chem. Soc.* **125** 13318
[30] Yoo S, Zhao J J, Wang J L and Zeng X C 2004 *J. Am. Chem. Soc.* **126** 13845
[31] Bai J, Cui L F, Wang J L, Yoo S, Li X, Jellinek J, Koehler C, Frauenheim T, Wang L S and Zeng X C 2006 *J. Phys. Chem.* A **110** 908
[32] Yoo S and Zeng X C 2006 *J. Chem. Phys.* **124** 054304
[33] Yoo S, Shao N, Koehler C, Fraunhaum T and Zeng X C 2006 *J. Chem. Phys.* **124** 164311
[34] Oña O, Bazterra V E, Caputo M C, Facelli J C, Fuentealba P and Ferraro M B 2006 *Phys. Rev.* A **73** 053203
[35] Bulusu S, Yoo S and Zeng X C 2005 *J. Chem. Phys.* **122** 164305
[36] Wang J L, Wang G H and Zhao J J 2001 *Phys. Rev.* B **64** 205411
[37] Ma S J and Wang G H 2006 *THEOCHEM* **767** 75
[38] Liang F S and Li B X 2004 *Phys. Lett.* A **328** 407
[39] Yoo S and Zeng X C 2006 *J. Chem. Phys.* **124** 184309
[40] Zhu X L, Zeng X C and Lei Y A 2004 *J. Chem. Phys.* **120** 8985
[41] Yoo S and Zeng X C 2005 *J. Chem. Phys.* **123** 164303
[42] Fuke K, Tsukamoto K, Misaizu F and Sanekata M 1993 *J. Chem. Phys.* **99** 7807
[43] Raghavachari K and Rohlfing C M 1987 *Chem. Phys. Lett.* **143** 428
[44] Shvartsburg A A, Jarrold M F, Liu B, Lu Z Y, Wang C Z and Ho K M 1998 *Phys. Rev. Lett.* **81** 4616
[45] Idrobo J C, Yang M and Jackson K A 2006 *Phys. Rev.* B **74** 153410
[46] Li B X and Cao P L 2000 *Phys. Rev.* B **62** 15788
[47] Yoo S and Zeng X C 2003 *J. Chem. Phys.* **119** 1442
[48] Zhu X L and Zeng X C 2003 *J. Chem. Phys.* **118** 3558
[49] Zhao L Z, Lu W C, Qin W, Wang C Z and Ho K H 2008 *J. Phys. Chem.* A **112** 5815
[50] Chuang F C, Wang C Z and Ho K H 2006 *Phys. Rev.* B **73** 125431
[51] Daven D M, Tit N, Morris J R and Ho K M 1996 *Chem. Phys. Lett.* **256** 195
[52] Frisch M J *et al* 2003 *Gaussian 03, Revision B* (Pittsburgh, PA: Gaussian)
[53] Martin T P and Schaber H 1985 *J. Chem. Phys.* **83** 855
[54] Rajesh C, Majumder C, Rajan M G R and Kulshreshtha S K 2005 *Phys. Rev.* B **72** 235411
[55] de Heer W A 1993 *Rev. Mod. Phys.* **65** 611
[56] Brack M 1993 *Rev. Mod. Phys.* **65** 677